Magnetic Reconnection and Pedestal Collapse During ELMs

J. P. Sauppe[1], C. R. Sovinec[1], X. Q. Xu[2], M. V. Umansky[2], I. Joseph[2]

[1]University of Wisconsin-Madison
[2]Lawrence Livermore National Laboratory

Fusion Energy Sciences

BOUT++
Boundary Plasma Turbulence Code

IM Release #: LLNL-PRES-512876

Using the BOUT++ plasma boundary turbulence code, we examine the role that hyper-resistivity plays in simulations of ELMs and the pedestal collapse.

- BOUT++ simulations achieved ELM pedestal collapse consistent with experiment after including several non-ideal effects, most notably a hyper-resistivity term
- Hyper-resistivity allows magnetic reconnection to occur on a different spatial scale than resistive reconnection
- To better understand the reconnection process, a new field-line tracing utility is developed for the BOUT++ framework
- Poincaré plots show that as the resistive layer width becomes smaller than the hyper-resistive layer width, the reconnection becomes independent of Lundquist number and core collapse is comparable to experiment

The physics module that is used solves the reduced MHD equations with several non-ideal effects included.

Reduced MHD Equations

Vorticity

$$\frac{\partial \varpi}{\partial t} + v_E \cdot \nabla \varpi = B_0^2 \nabla_{\parallel} \left(\frac{j_{\parallel}}{B_0} \right) + 2 b_0 \times \kappa \cdot \nabla p$$

Pressure

$$\frac{\partial P}{\partial t} + v_E \cdot \nabla P = 0$$

Ohm's

$$\frac{\partial A_{\parallel}}{\partial t} = -\nabla_{\parallel} (\phi + \Phi_0) + \frac{\eta}{\mu_0} \nabla_{\perp}^2 A_{\parallel} - \frac{\eta_H}{\mu_0} \nabla_{\perp}^4 A_{\parallel}$$

Definitions

$$\varpi = \frac{n_0 M_i}{B_0} \left(\nabla_{\perp}^2 \phi + \frac{1}{n_0 Z_i e} \nabla_{\perp}^2 p_i \right), \quad P = P_0 + p$$

$$j_{\parallel} = J_{\parallel 0} - \frac{1}{\mu_0} \nabla_{\perp}^2 A_{\parallel}, \quad v_E = \frac{1}{B_0} b_0 \times \nabla (\phi + \Phi_0)$$

Non-ideal physics

✓Using resistive MHD term, resistivity can be renormalized as **Lundquist** Number

$$S = \mu_0 R v_A / \eta$$

✓Using hyper-resistivity η_H

$$S_H = \mu_0 R^3 v_A / \eta_H = S / \alpha_H$$

✓After gyroviscous cancellation, the diamagnetic drift modifies the vorticity and additional nonlinear terms

✓Using force balance and assuming no net rotation,

$$E_{r0} = (1/N_i Z_i e) \nabla_{\perp} P_{i0}$$

Ref: Xu et. al. PRL **105**, 175005 (2010)

Hyper-resistivity can allow reconnection to occur on coarser spatial scales resulting in magnetic reconnection that is independent of S.

- The resistive current layer is proportional to the square root of the plasma resistivity

$$\Delta_J \approx R_0 \sqrt{\frac{\omega_A}{\gamma_{PB} S}} \qquad S \equiv \frac{\mu_0 R_0 v_A}{\eta}$$

- The hyper-resistivity has a much stronger scaling with the hyper-Lundquist number, allowing reconnection on scales independent of S for sufficiently high S_H

$$\Delta_H \approx R_0 \left(\frac{\omega_A}{\gamma_{PB} S_H} \right)^{1/4} \qquad S_H = \frac{S}{\alpha_H}, \; \alpha_H \equiv \frac{\eta_H}{R_0^2 \eta} \approx 10^{-4} - 10^{-6}$$

- This stronger scaling makes nonlinear simulations at realistic S more tractable provided that the layer width is larger than the grid spacing

$$\Delta_H \geq \Delta_X >> \Delta_J$$

Including the hyper-resistivity in BOUT++ simulations shows pedestal collapse is limited to the edge and the energy lost is consistent with experiment.

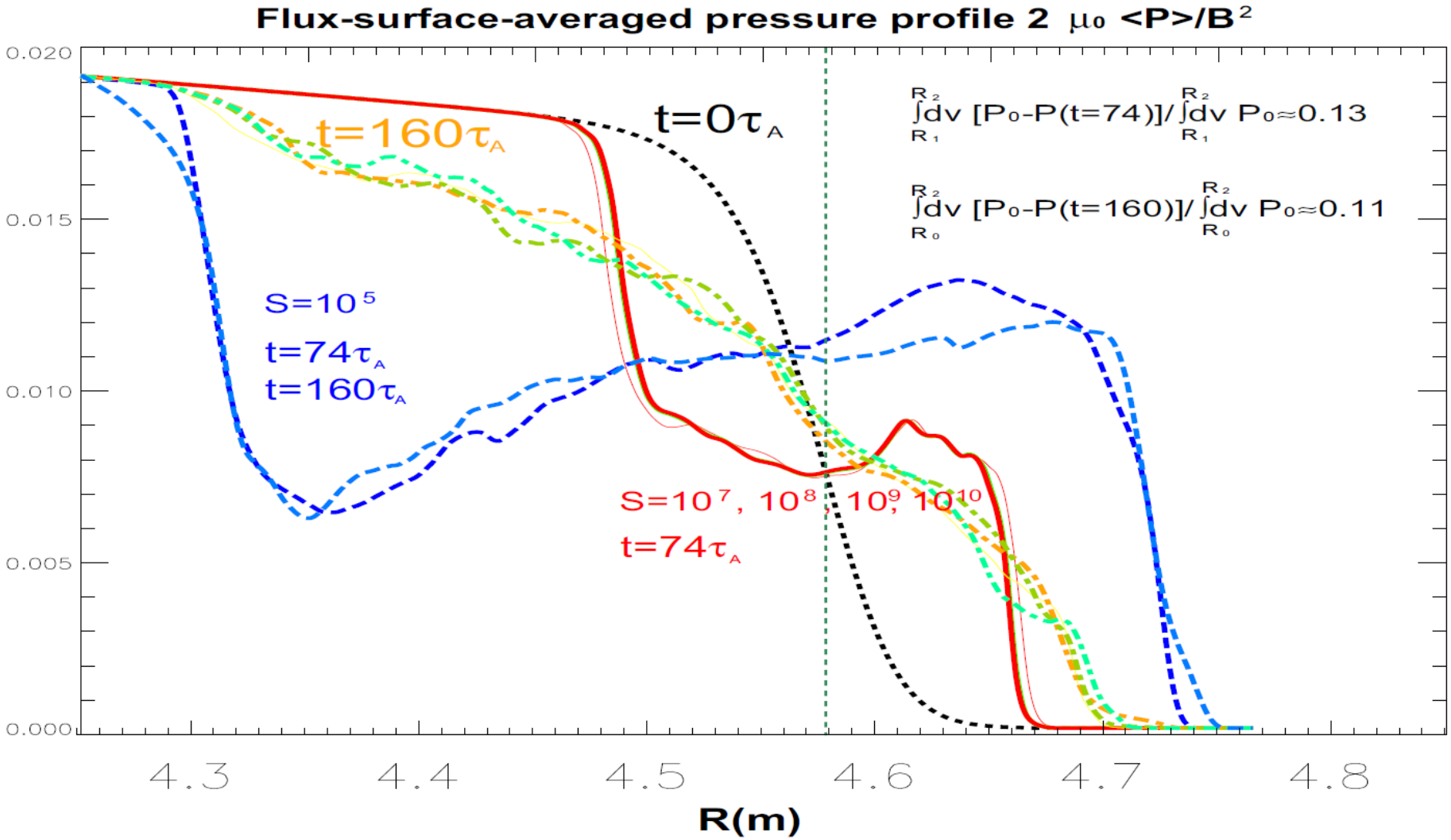

Ref: Xu et. al. PRL **105**, 175005 (2010)

We use a well-studied circular cross-section toroidal equilibrium generated by the TOQ equilibrium code (cbm18_dens8).

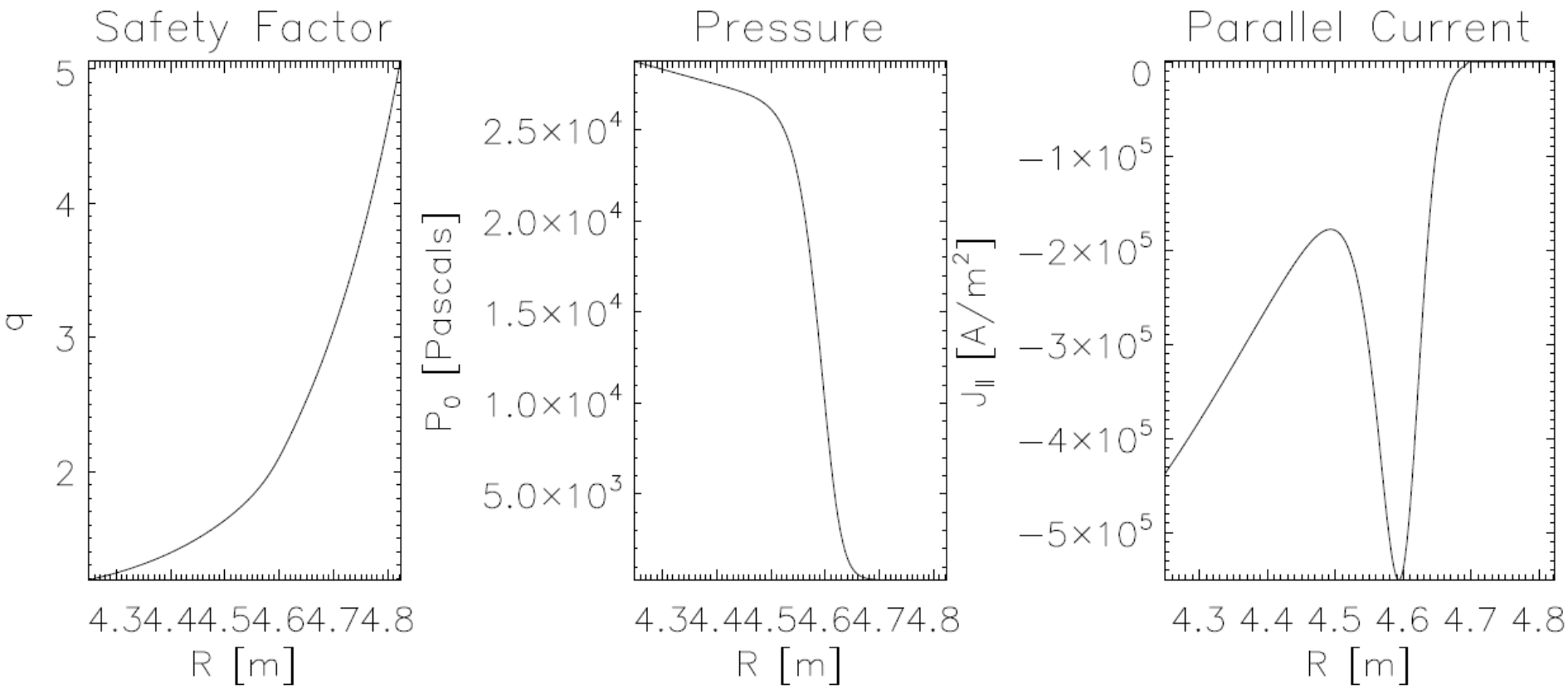

BOUT++ utilizes a coordinate system aligned with the magnetic field for computational efficiency.

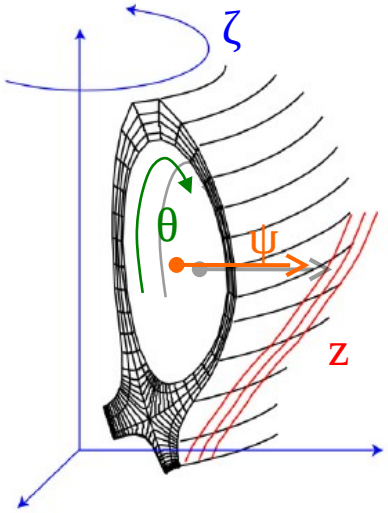

Field-aligned coordinates

$$x = \psi - \psi_0,$$

$$y = \theta,$$

$$z = \zeta - \int_{\theta_0}^{\theta} \nu(\psi,\theta)\, d\theta$$

where ν is the local safety factor given by: $\nu(\psi,\theta) = \dfrac{\vec{B}\cdot\nabla\zeta}{\vec{B}\cdot\nabla\theta}$

In most simulations, only a fraction of the torus is simulated

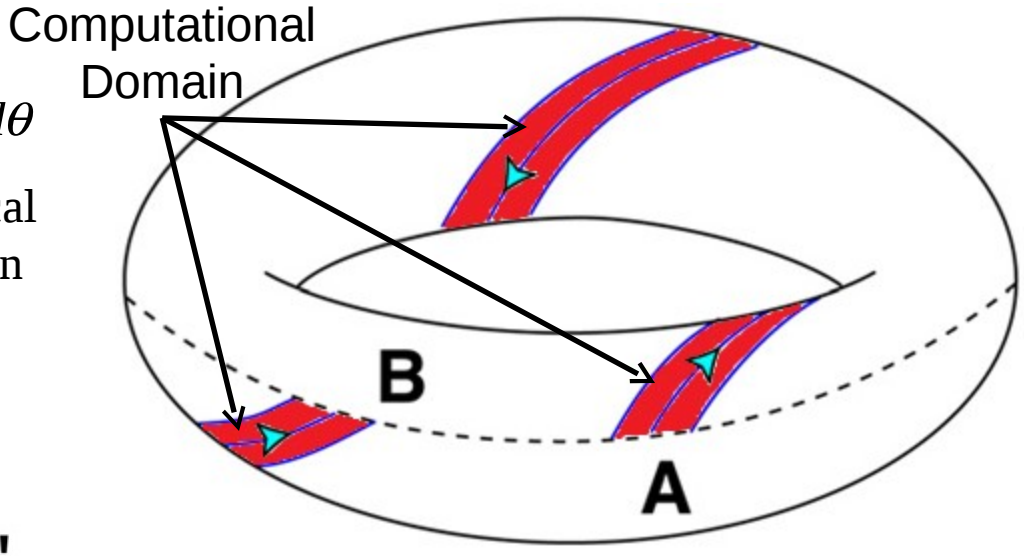

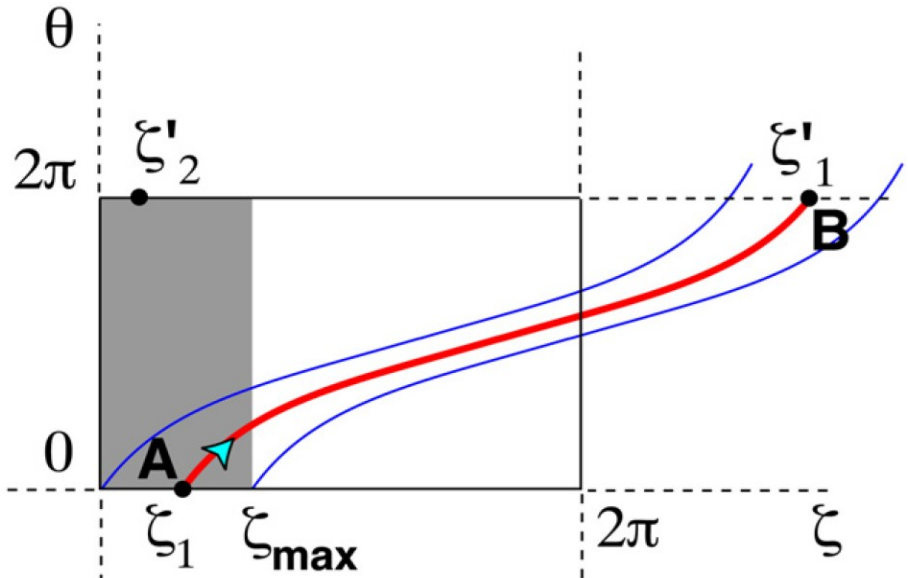

The y-periodicity requires a **twist-shift** condition due to the field-aligned system

$$F(x, y = 2\pi, z_0) = F(x, y = 0, z_1)$$

$$z_1 = \left(z_0 + \oint \nu dy\right) \text{MOD } z_{\max}$$

To analyze the reconnection process, Poincaré plots are created by integrating along the field lines using the appropriate twist-shift boundary conditions.

To produce a Poincaré plot on a poloidal plane $y = y_0$

1) Integrate from $y = y_0$ to $y = 2\pi$
2) Use twist-shift to jump from $y = 2\pi$ to $y = 0$
3) Integrate from $y = 0$ to $y = y_0$

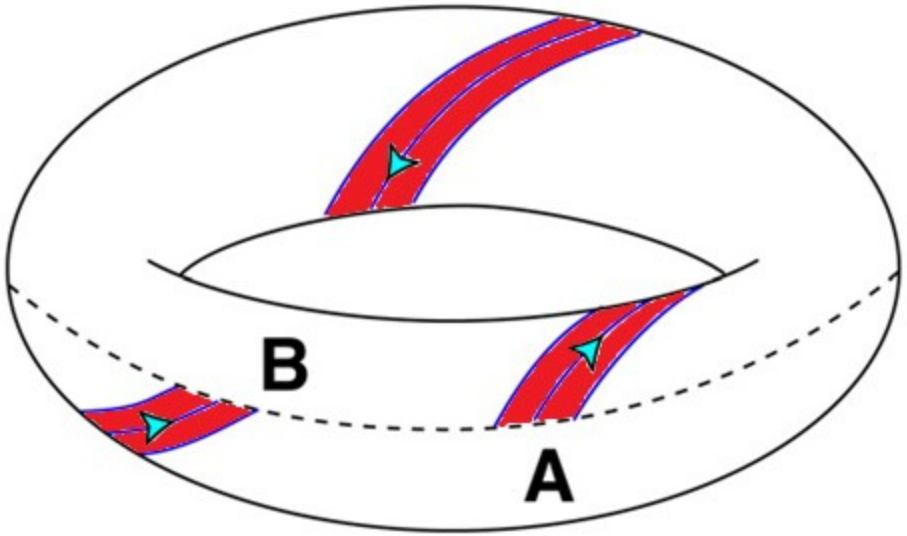

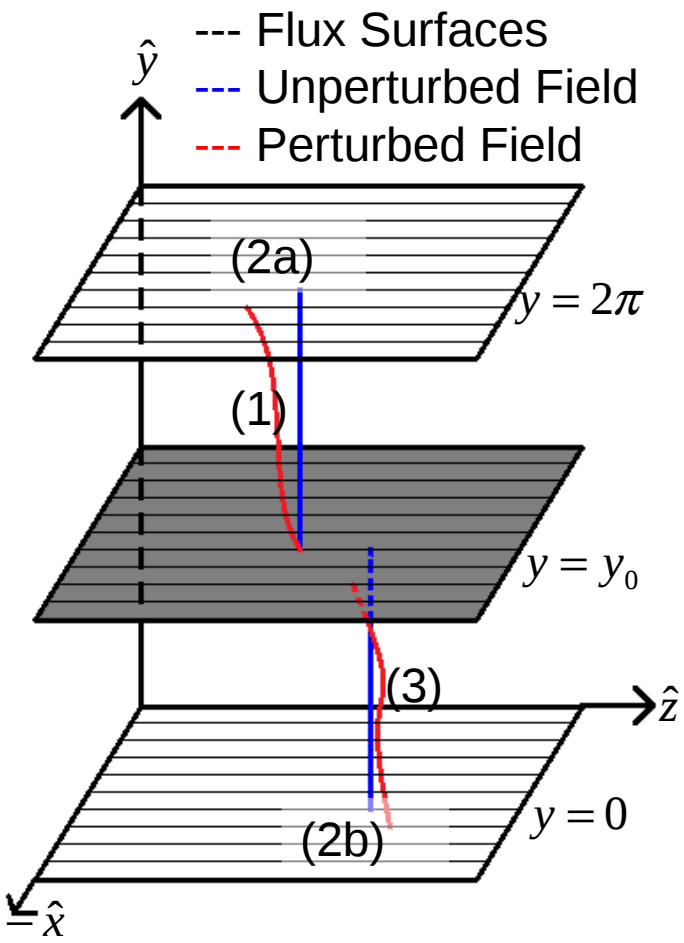

The field-line equations depend upon the perturbed vector potential everywhere, but BOUT++ solves for discrete points.

- In BOUT++, the perturbed parallel vector potential is evolved

$$\tilde{\vec{B}} = \vec{\nabla} \times \left(\tilde{A}_{\parallel} \hat{b}_0 \right)$$

- The field-line equations in the BOUT++ coordinate system become

$$\frac{dx}{dy} = \frac{\frac{1}{B_0}\left[\left(g^{13}g^{21} - g^{11}g^{23}\right)\frac{\partial \tilde{A}_{\parallel}}{\partial y} + \left(g^{13}g^{31} - g^{11}g^{33}\right)\frac{\partial \tilde{A}_{\parallel}}{\partial z}\right] + \tilde{A}_{\parallel}\left(\left(\hat{\boldsymbol{b}}_0 \times \boldsymbol{\kappa}\right) \cdot \boldsymbol{\nabla} x\right)}{\frac{B_\theta}{h_\theta} + \frac{1}{B_0}\left[\left(g^{23}g^{11} - g^{21}g^{13}\right)\frac{\partial \tilde{A}_{\parallel}}{\partial x} + \left(g^{23}g^{31} - g^{21}g^{33}\right)\frac{\partial \tilde{A}_{\parallel}}{\partial z}\right] + \tilde{A}_{\parallel}\left[\left(\hat{\boldsymbol{b}}_0 \times \boldsymbol{\kappa}\right) \cdot \boldsymbol{\nabla} y + \frac{B_\theta}{h_\theta}\frac{\mu_0}{B_0^2} J_{\parallel,0}\right]}$$

$$\frac{dz}{dy} = \frac{\frac{1}{B_0}\left[\left(g^{33}g^{11} - g^{31}g^{13}\right)\frac{\partial \tilde{A}_{\parallel}}{\partial x} + \left(g^{33}g^{21} - g^{31}g^{23}\right)\frac{\partial \tilde{A}_{\parallel}}{\partial y}\right] + \tilde{A}_{\parallel}\left(\left(\hat{\boldsymbol{b}}_0 \times \boldsymbol{\kappa}\right) \cdot \boldsymbol{\nabla} z\right)}{\frac{B_\theta}{h_\theta} + \frac{1}{B_0}\left[\left(g^{23}g^{11} - g^{21}g^{13}\right)\frac{\partial \tilde{A}_{\parallel}}{\partial x} + \left(g^{23}g^{31} - g^{21}g^{33}\right)\frac{\partial \tilde{A}_{\parallel}}{\partial z}\right] + \tilde{A}_{\parallel}\left[\left(\hat{\boldsymbol{b}}_0 \times \boldsymbol{\kappa}\right) \cdot \boldsymbol{\nabla} y + \frac{B_\theta}{h_\theta}\frac{\mu_0}{B_0^2} J_{\parallel,0}\right]}$$

- The vector potential, its spatial derivatives, and the metric coefficients must be determined at all points in the domain

Two interpolation methods that preserve the continuity of first derivatives across cell boundaries are implemented.

- The first method uses a bicubic interpolant in x and y with a Fourier representation for the periodic binormal direction z

$$f(x,y,z) = a_0(x,y) + \sum_{k=1}^{N} \left[a_k(x,y)\cos(kz) + b_k(x,y)\sin(kz) \right]$$

$$a_k(x,y) = \sum_{i,j=0}^{3} (a_k)_{i,j}\, x^i y^j \qquad b_k(x,y) = \sum_{i,j=0}^{3} (b_k)_{i,j}\, x^i y^j$$

- The second method uses a tricubic interpolant

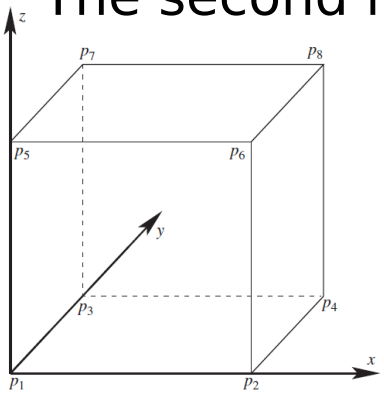

$$f(x,y,z) = \sum_{i,j,k=0}^{3} a_{i,j,k} x^i y^j z^k$$

  - Coefficients chosen so that $\left\{ f, \frac{\partial f}{\partial x}, \frac{\partial f}{\partial y}, \frac{\partial f}{\partial z}, \frac{\partial^2 f}{\partial x \partial y}, \frac{\partial^2 f}{\partial x \partial z}, \frac{\partial^2 f}{\partial y \partial z}, \frac{\partial^3 f}{\partial x \partial y \partial z} \right\}$ matches at the corners

Ref: Lekien & Marsden, Int. J. Numer. Meth. Engng 2005; **63**:455–471

Using a model function, both methods correctly capture the primary q=m/5 island structures.

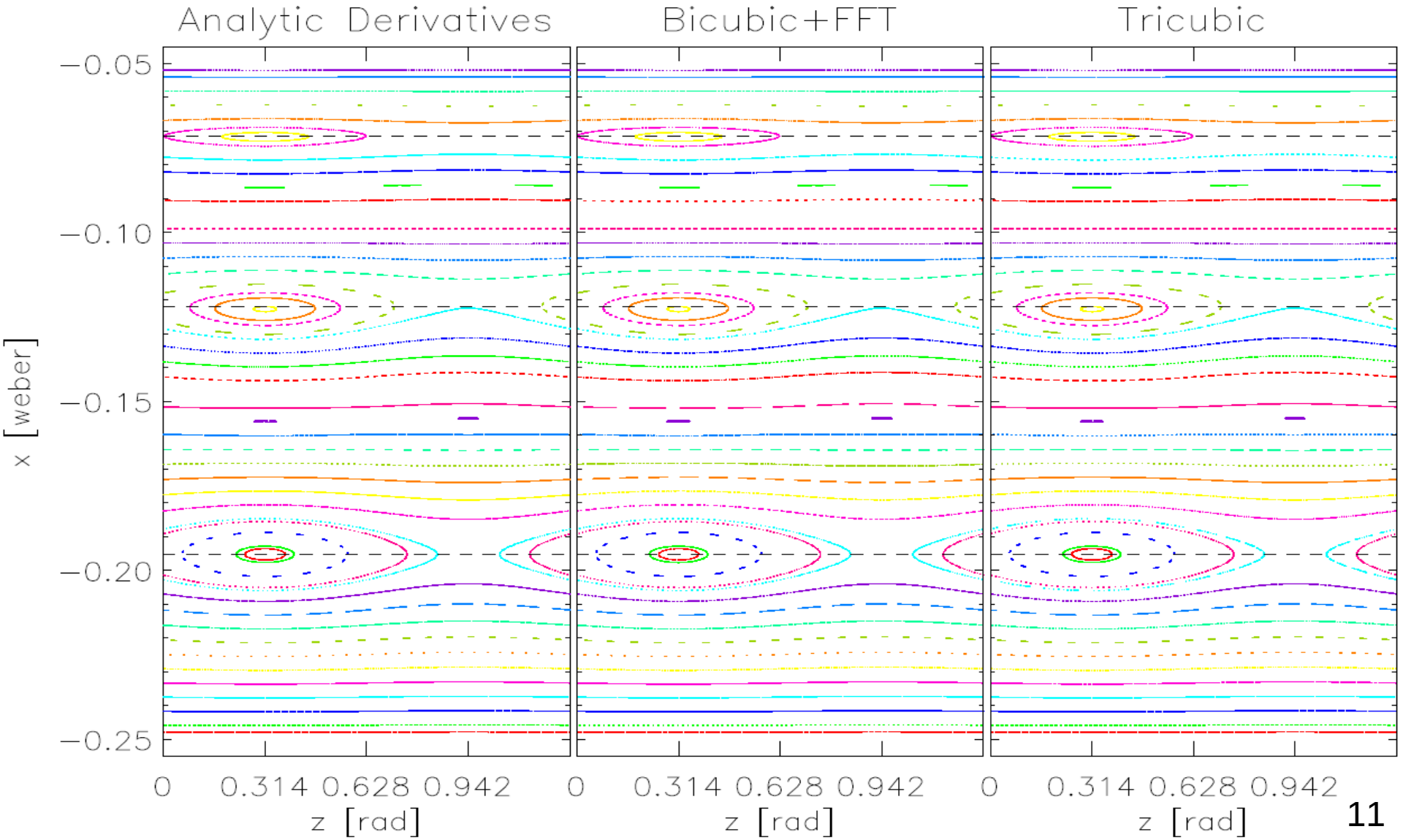

The islands grow and secondary islands form as the perturbation increases.

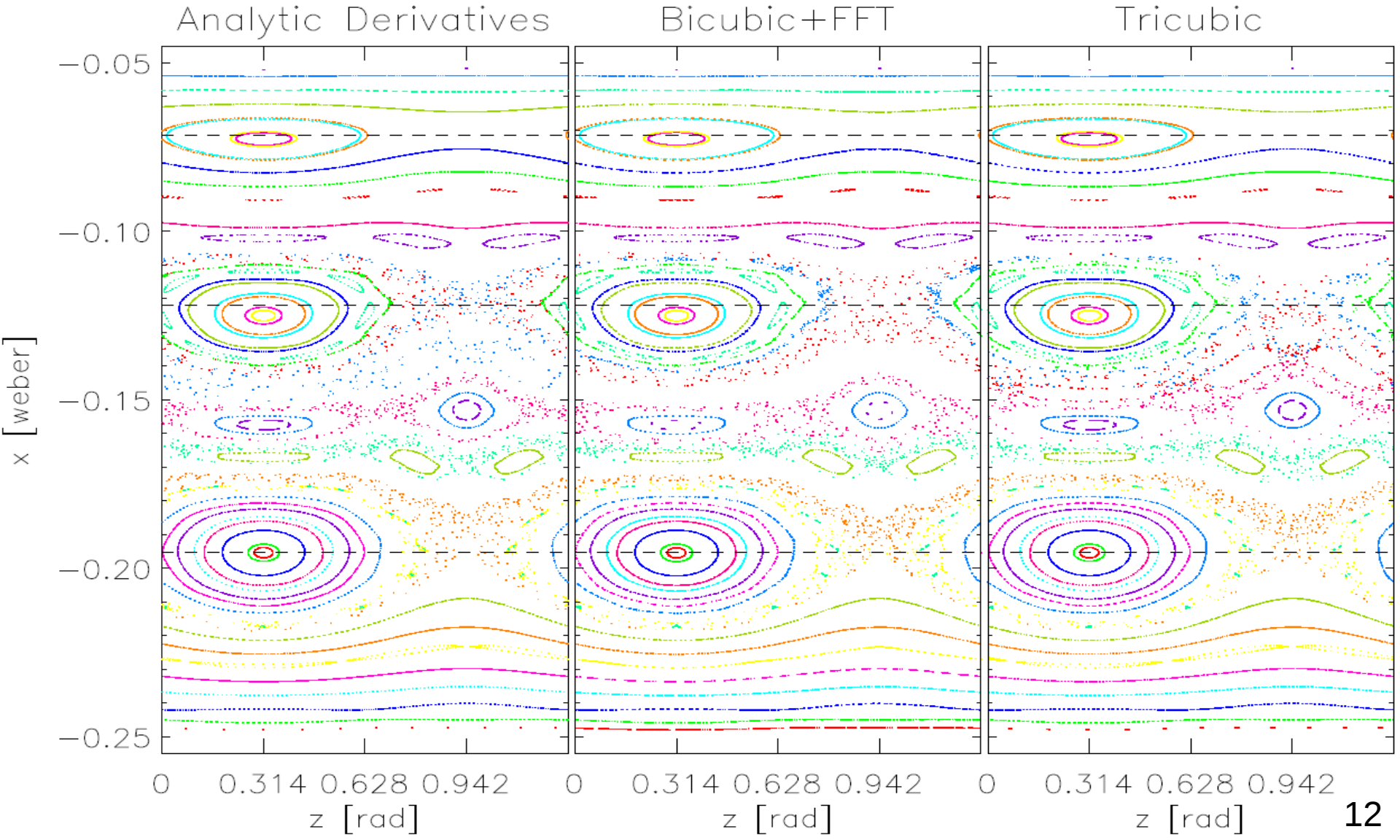

Stochastic regions develop when the secondary islands begin to overlap.

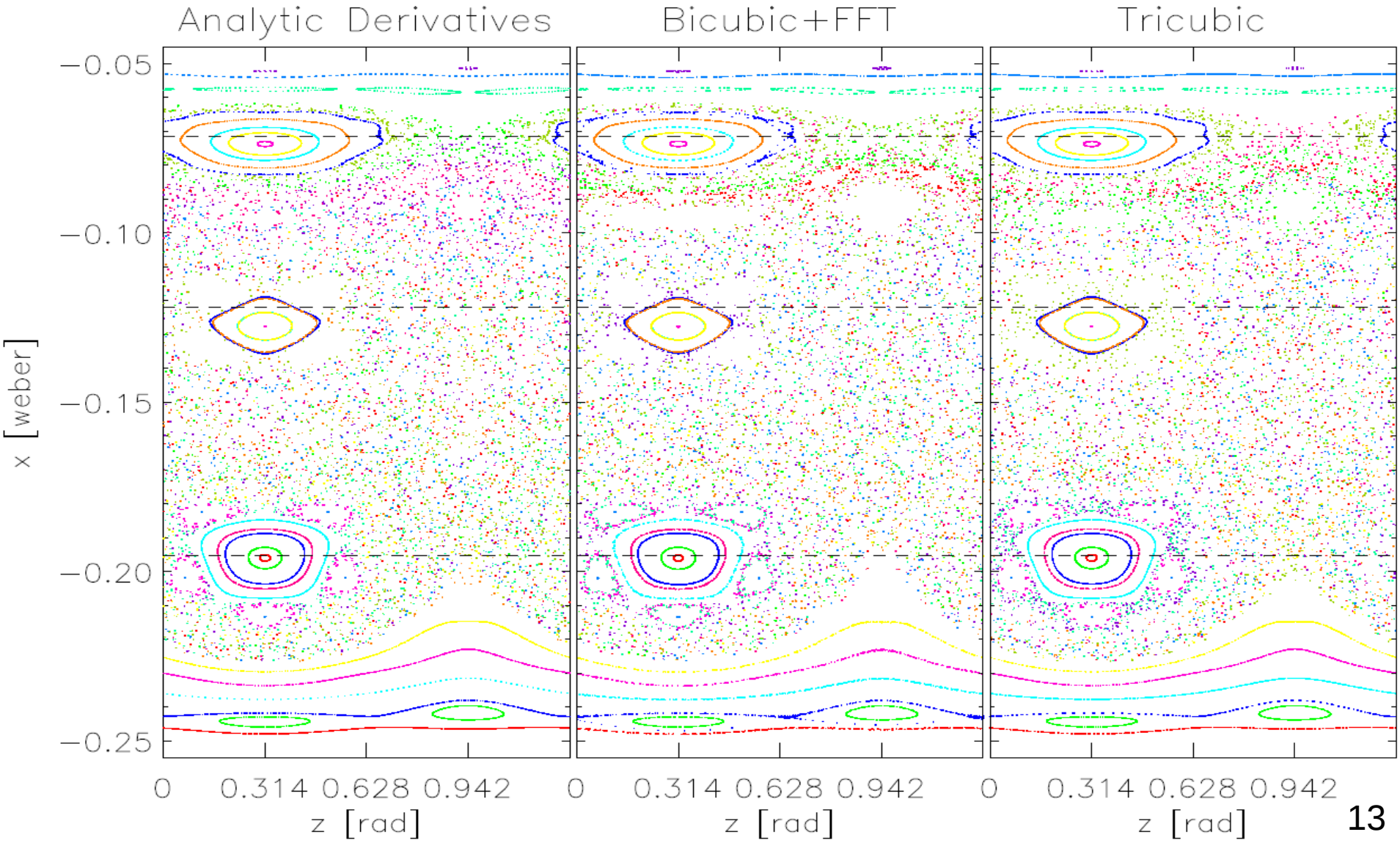

For a single high toroidal mode (k_z=60), bicubic+FFT interpolation appears better at resolving the topology.

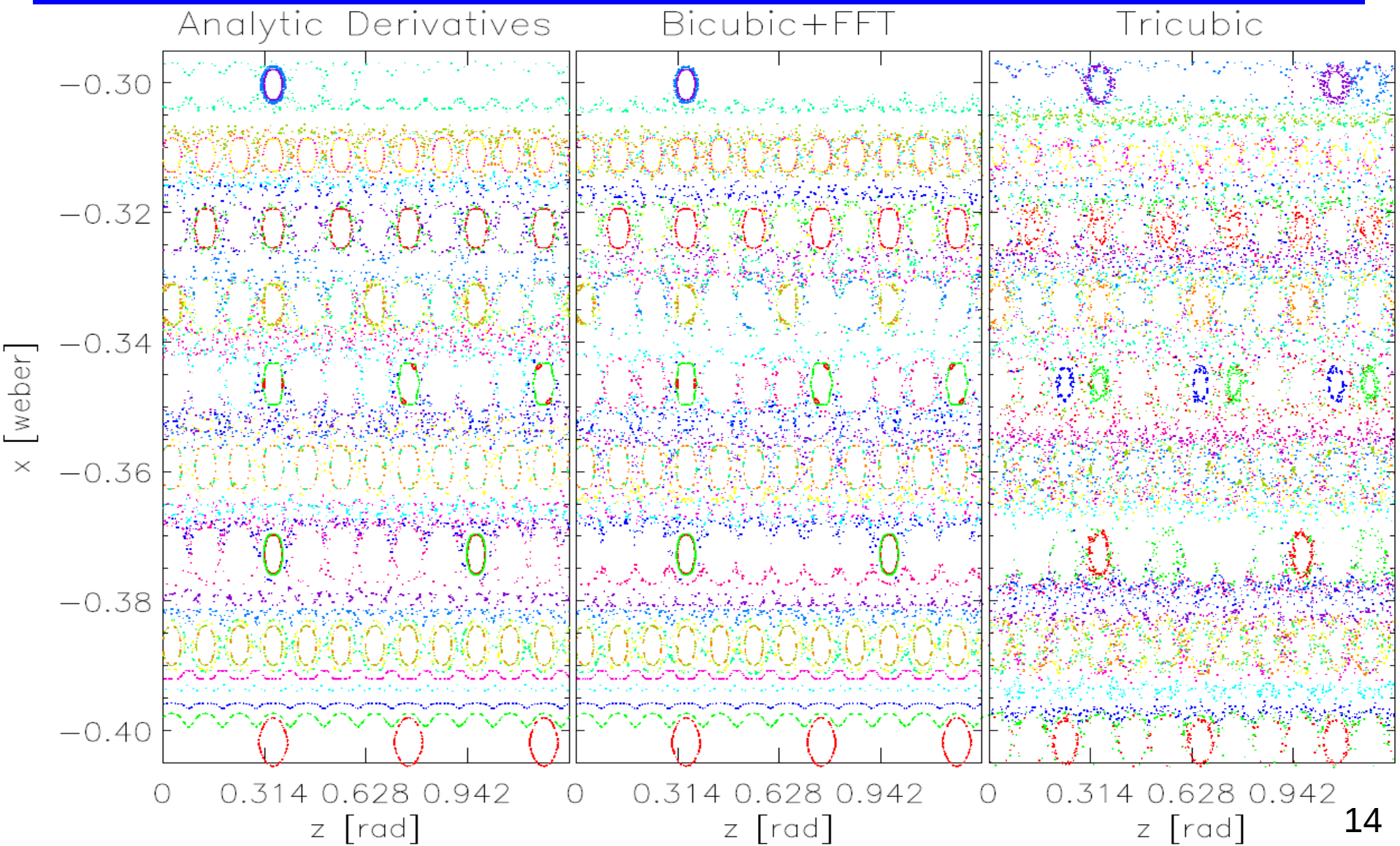

Data from BOUT++ simulations in the early non-linear phase exhibit unphysical attractors for the bicubic+FFT interpolation but not the tricubic interpolation.

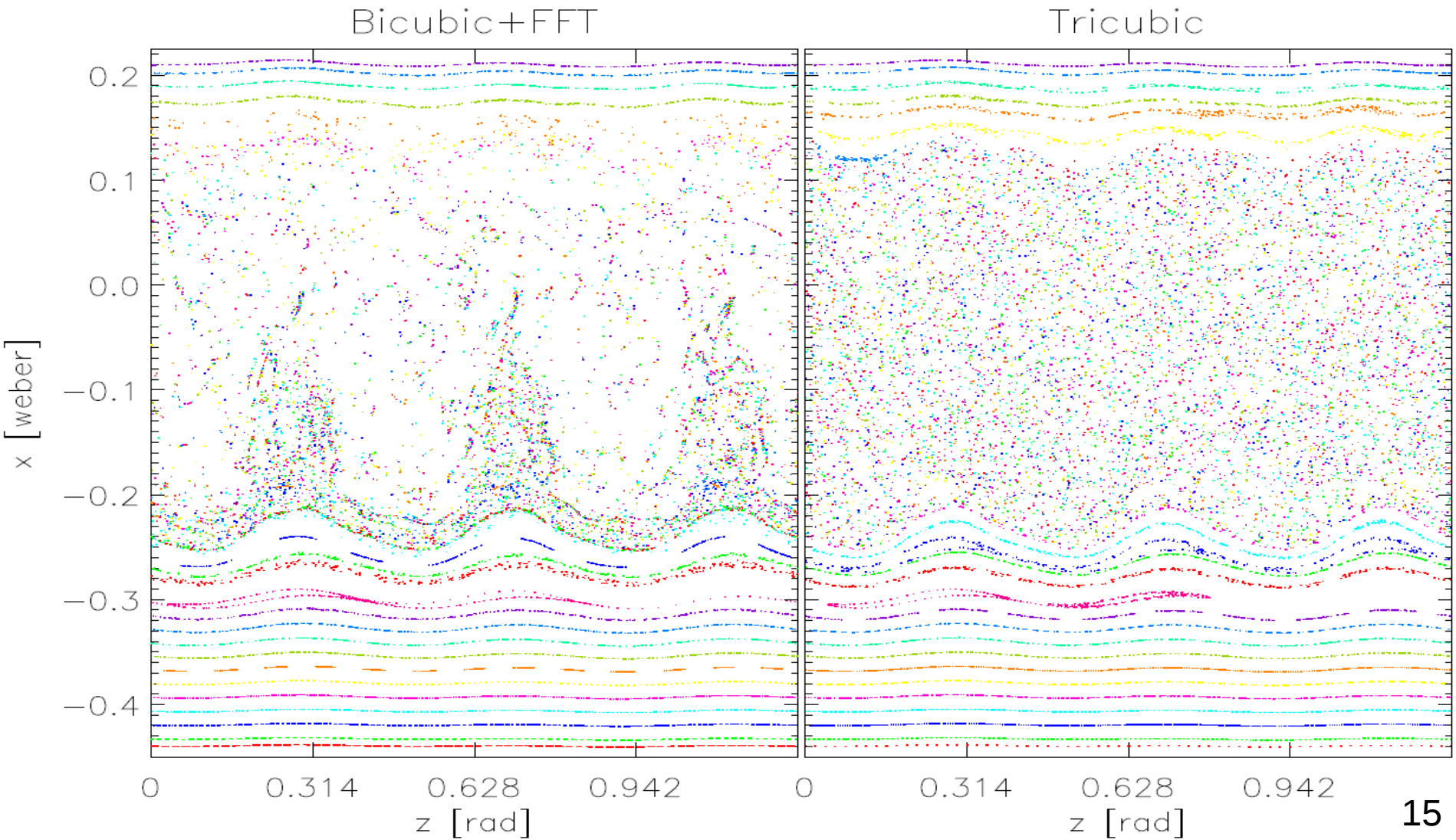

For $S=10^8$, $S_H=10^{12}$, the reconnection region is small and the collapse is limited.

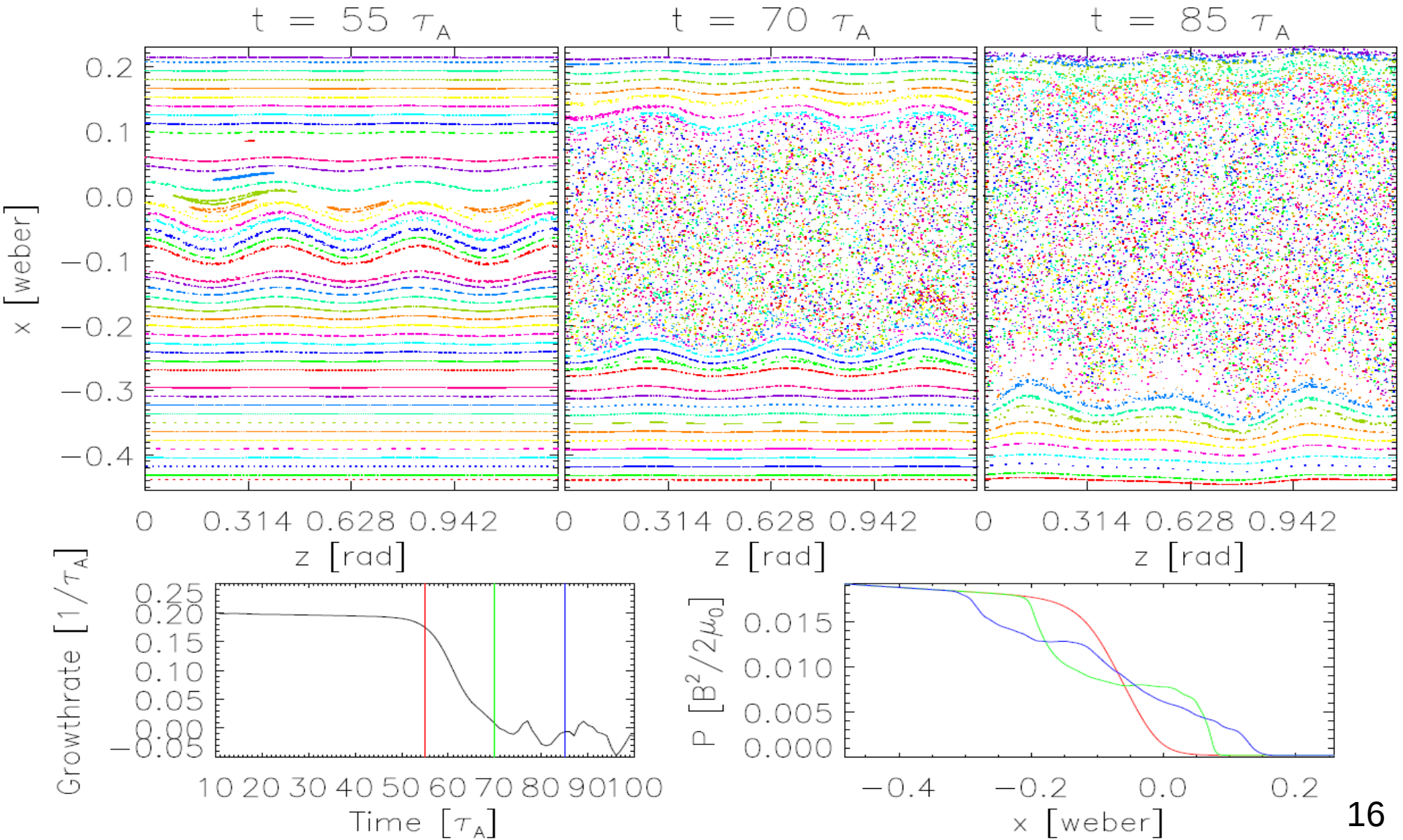

Changing S ($S=10^7$, $S_H=10^{12}$) has little effect if hyper-resistive reconnection is dominant.

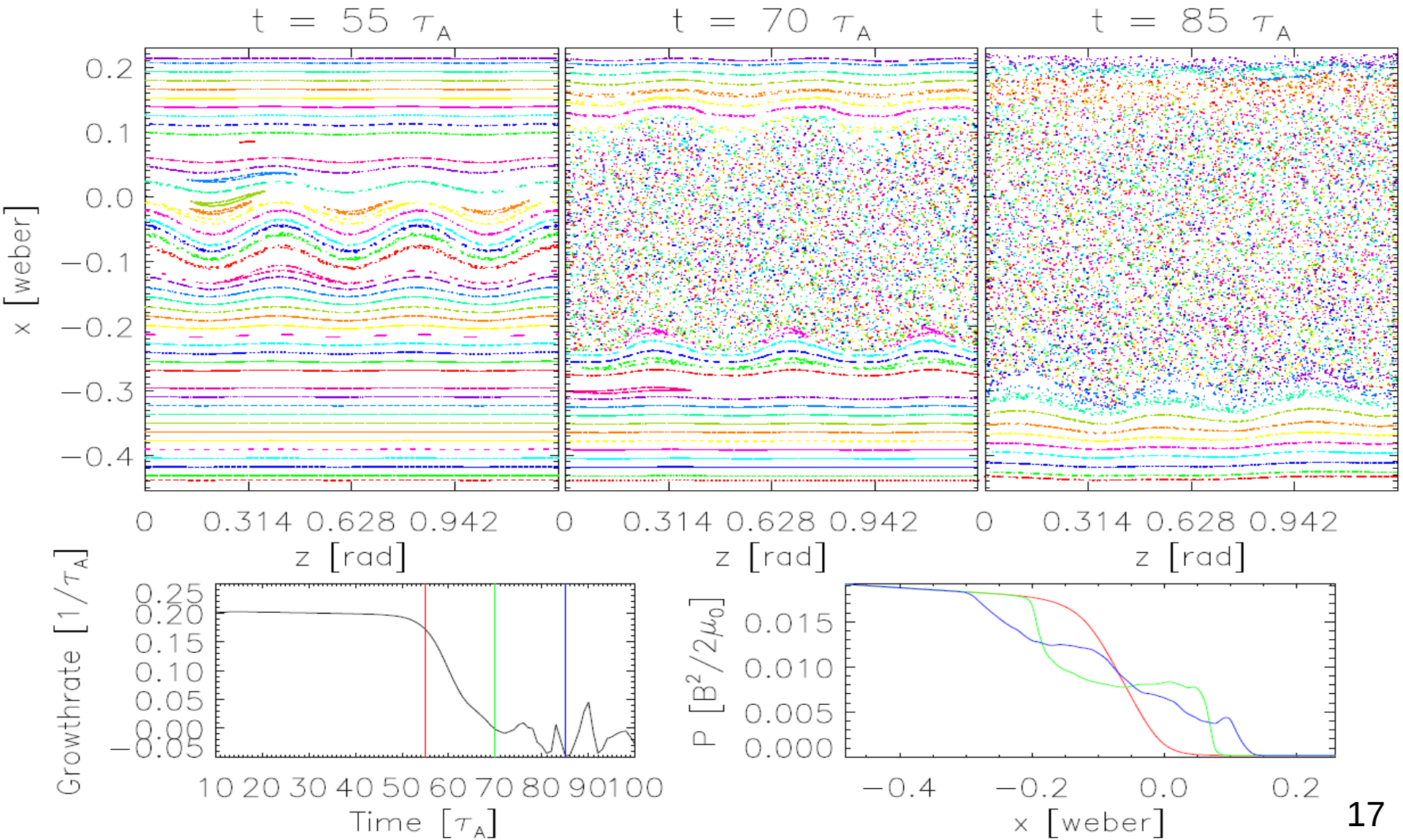

When $S=10^6, S_H=10^{12}$ resistive reconnection begins to dominate ($\Delta_J > \Delta_H$) and the pedestal crash is larger.

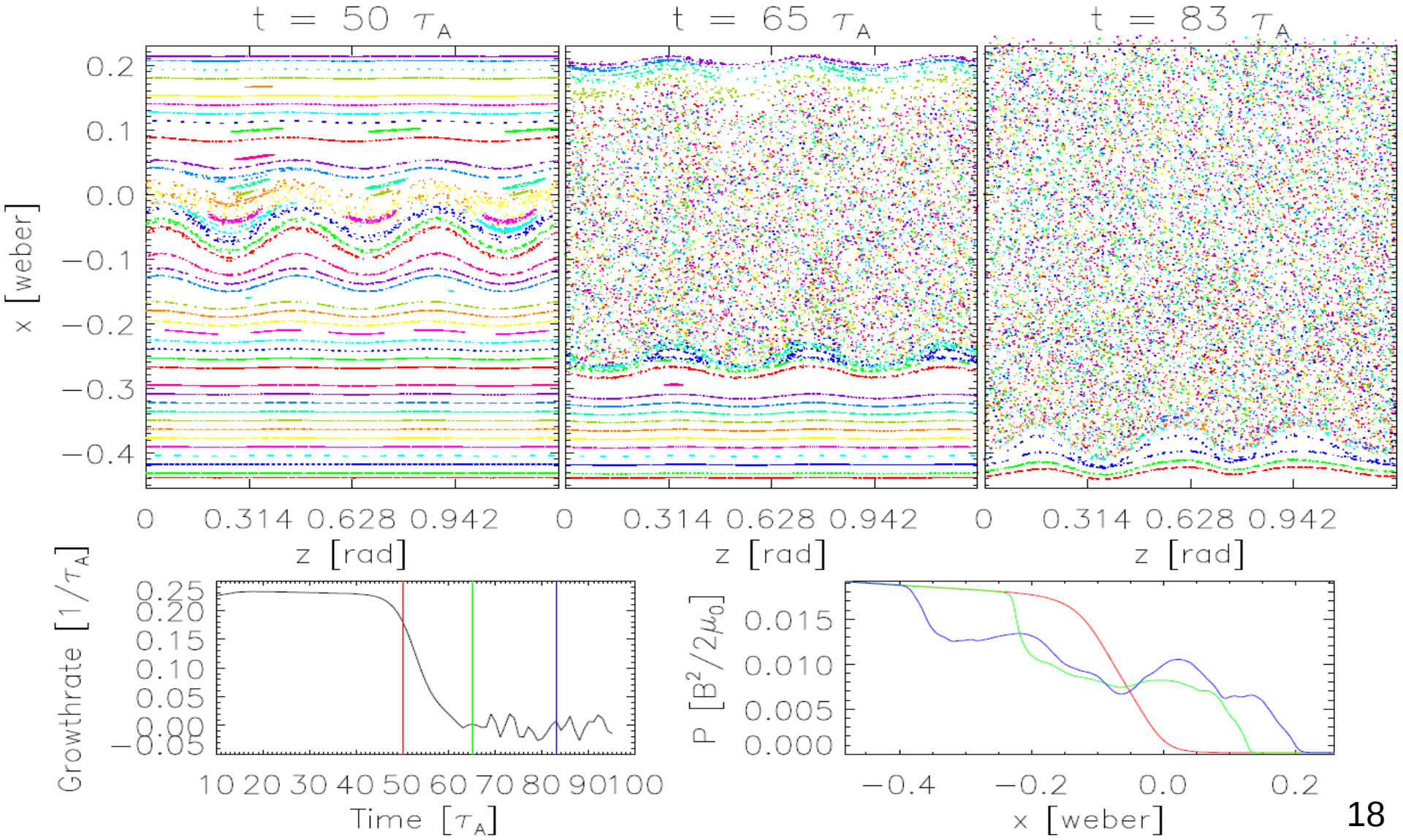

The pedestal collapse is governed by the larger reconnection layer width.

- The size of the ELM can be estimated as

$$\Delta_{ELM} \equiv \frac{\left\langle \int_{R_{out}}^{R_{in}} dR \oint d\theta \left(P_0 - \langle P \rangle_\zeta \right) \right\rangle_t}{\int_{R_{out}}^{R_{in}} dR \oint d\theta P_0}$$

The time average is over the ELM crash period, typically ~50-100 τ_A

	$S=10^5$ **Δ_J~34.0 mm**	**$S=10^6$** **Δ_J~10.7 mm**	**$S=10^7$** **Δ_J~3.40 mm**	**$S=10^8$** **Δ_J~1.07 mm**
$S_H=10^{11}$ **Δ_H~10.7 mm**	Δ_{ELM}=23.5% <t>=42-92 τ_A	Δ_{ELM}=12.1% <t>=45-95 τ_A	Δ_{ELM}=8.06% <t>=47-97 τ_A	Δ_{ELM}=10.8% <t>=50-100 τ_A
$S_H=10^{12}$ **Δ_H~6.05 mm**	Δ_{ELM}=20.8% <t>=45-70 τ_A	Δ_{ELM}=7.29% <t>=45-95 τ_A	Δ_{ELM}=3.48% <t>=50-100 τ_A	Δ_{ELM}=3.43% <t>=50-100 τ_A

Topology changes in an ideal MHD case run with BOUT++ suggest that numerical dissipation in the code may be an issue.

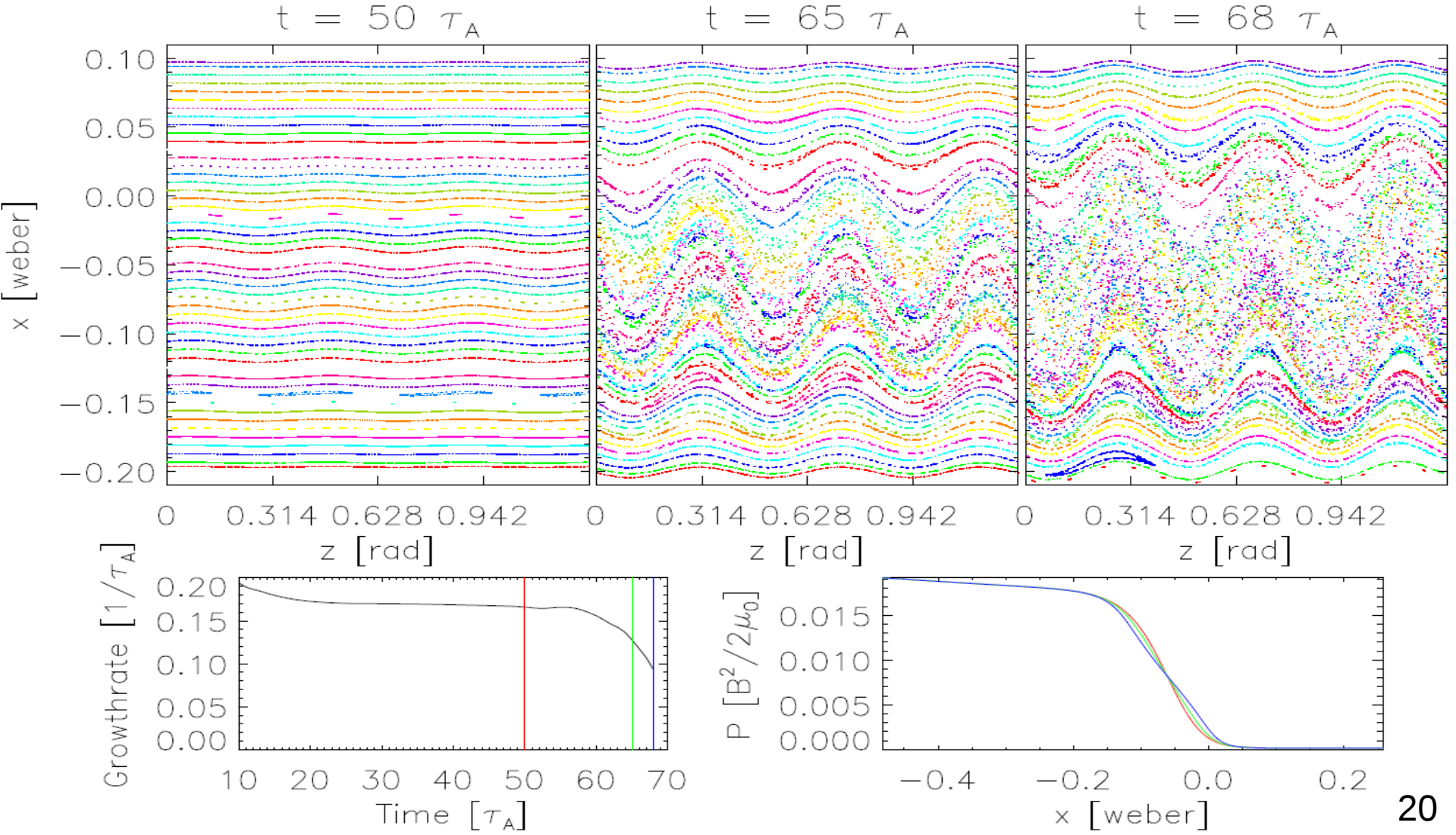

Conclusions

- A line-tracing utility was implemented for post-processing BOUT++ simulation results to produce Poincaré plots and analyze the magnetic topology
  - Bicubic+FFT interpolation does better for high modes
  - Tricubic does not suffer from attractors in field-line plots

- When the hyper-resistive layer width is larger than the resistive layer width, hyper-resistive reconnection dominates the dynamics and the resulting pedestal collapse is independent of S
  - Sufficiently high S_H ($>10^{11}$) with realistic S ($\sim 10^7$-10^8) leads to ELM sizes that match experimental ones